PNAS RESEARCH ARTICLE | NEUROSCIENCE

Disruption of *Cdh23* exon 68 splicing leads to progressive hearing loss in mice by affecting tip-link stability

Nana Li[a,1], Shuang Liu[b,1], Dange Zhao[c,1], Haibo Du[a], Yuehui Xi[a], Xiaoxi Wei[c], Qingling Liu[b], Ulrich Müller[d], Qing Lu[c,2], Wei Xiong[b,2], and Zhigang Xu[a,e,2]

Edited by Jeremy Nathans, Johns Hopkins University School of Medicine, Baltimore, MD; received June 13, 2023; accepted December 21, 2023

Inner ear hair cells are characterized by the F-actin-based stereocilia that are arranged into a staircase-like pattern on the apical surface of each hair cell. The tips of shorter-row stereocilia are connected with the shafts of their neighboring taller-row stereocilia through extracellular links named tip links, which gate mechano-electrical transduction (MET) channels in hair cells. Cadherin 23 (CDH23) forms the upper part of tip links, and its cytoplasmic tail is inserted into the so-called upper tip-link density (UTLD) that contains other proteins such as harmonin. The *Cdh23* gene is composed of 69 exons, and we show here that exon 68 is subjected to hair cell–specific alternative splicing. Tip-link formation is not affected in genetically modified mutant mice lacking *Cdh23* exon 68. Instead, the stability of tip links is compromised in the mutants, which also suffer from progressive and noise-induced hearing loss. Moreover, we show that the cytoplasmic tail of CDH23(+68) but not CDH23(−68) cooperates with harmonin in phase separation–mediated condensate formation. In conclusion, our work provides evidence that inclusion of *Cdh23* exon 68 is critical for the stability of tip links through regulating condensate formation of UTLD components.

CDH23 | alternative splicing | hair cells | tip links | mechano-electrical transduction

Significance

Mechano-electrical transduction (MET) in inner ear hair cells requires tip links, which are formed by single-transmembrane proteins cadherin 23 (CDH23) and protocadherin 15 (PCDH15). The *Cdh23* gene is subjected to alternative splicing and exon 68 is specifically included in the inner ear. The physiological significance of this tissue-specific splicing of *Cdh23* exon 68 has remained elusive. Here, we show that *Cdh23* exon 68 is necessary for maintaining tip-link stability, and mice with a *Cdh23* exon 68 deletion suffer from progressive and noise-induced hearing loss. We also provide evidence that exon 68 regulates CDH23 homodimerization and condensate formation with harmonin, a cytoplasmic binding partner for CDH23 that is concentrated at the tip-link insertion point near CDH23.

As the mechanosensitive receptor cells in the inner ear, hair cells are characterized by their hair bundles on the apical cell surface. The hair bundle of each hair cell consists of one tubulin-based kinocilium and dozens of F-actin-based stereocilia that are organized in rows of increasing height (1). The kinocilium plays an important role in hair bundle development, is lost in mature cochlear hair cells, and is dispensable for mechano-electrical transduction (MET) (1–3). In contrast, stereocilia are essential for MET by hair cells (2). Various types of extracellular links such as tip links, lateral links, ankle links, and kinocilial links connect stereocilia to each other as well as to the kinocilium (4–6). Tip links are essential for MET and connect the tips of shorter-row stereocilia with the shafts of neighboring taller-row stereocilia (4, 6, 7). When mechanical force deflects stereocilia toward the taller edge of the hair bundle, the tension in tip links is thought to increase, which in turn affects the open probability of MET channels localized near the lower end of tip links, resulting in the influx of cations into hair cells (2, 8, 9).

Two single-transmembrane cadherins, cadherin 23 (CDH23) and protocadherin 15 (PCDH15), are essential components of lateral links, kinocilial links, and tip links (10–16). In tip links, CDH23 and PCDH15 form cis-homodimers through lateral interaction and trans-interact with each other via their N-terminal extracellular cadherin (EC) domains, forming the upper and lower part of tip links, respectively (Fig. 1*A*) (12). Mutations in *CDH23* and *PCDH15* cause syndromic and non-syndromic hearing loss in human (17–20). Mutations in their orthologous mouse genes also cause hearing impairment that is associated with deficits in the stereocilia morphology and tip-link formation and function (21–23). The upper and lower ends of tip links are anchored at the stereociliary membrane within electron-dense plaques referred to as upper tip-link density (UTLD) and lower tip-link density (LTLD), respectively (Fig. 1*A*) (5, 24). Immunolocalization studies have revealed that UTLD components include Myosin VIIA (MYO7A), SANS, and harmonin in addition to the cytoplasmic tail of CDH23 (25, 26). Recently, it was suggested that MYO7A, SANS, and harmonin may form the UTLD via phase separation (27).

Transcription from different transcriptional start sites produces three main CDH23 isoforms, namely CDH23-V1 and CDH23-V2 with 27 and 7 extracellular EC domains, respectively, and CDH23-V3, which is a cytosolic protein (Fig. 1*B*) (13). Moreover, the *Cdh23* gene contains 69 exons, and exon 68 is subjected to alternative splicing giving rise to two CDH23 isoforms, CDH23(+68) and CDH23(−68) (Fig. 1*B*) (10, 13, 28). *Cdh23* is expressed in multiple tissues, whereas exon 68 inclusion has so far only been detected in the inner ear (29). Exon 68 is 105 base pairs (bp) long, encoding a peptide of 35 amino acids in the cytoplasmic tail of CDH23, which regulates the interaction of CDH23 with

Author contributions: Z.X. designed research; N.L., S.L., D.Z., H.D., Y.X., X.W., and Q. Liu performed research; N.L., S.L., U.M., Q. Lu, W.X., and Z.X. analyzed data; and N.L., U.M., Q. Lu, W.X., and Z.X. wrote the paper.

Competing interest statement: Author U.M. and Editor J.N. are at the same institution but have not collaborated directly.

This article is a PNAS Direct Submission.

[1]N.L., S.L., and D.Z. contributed equally to this work.

[2]To whom correspondence may be addressed. Email: luqing67@sjtu.edu.cn, wei_xiong@cibr.ac.cn, or xuzg@sdu.edu.cn.

This article contains supporting information online at https://www.pnas.org/lookup/suppl/doi:10.1073/pnas.2309656121/-/DCSupplemental.

Published February 26, 2024.

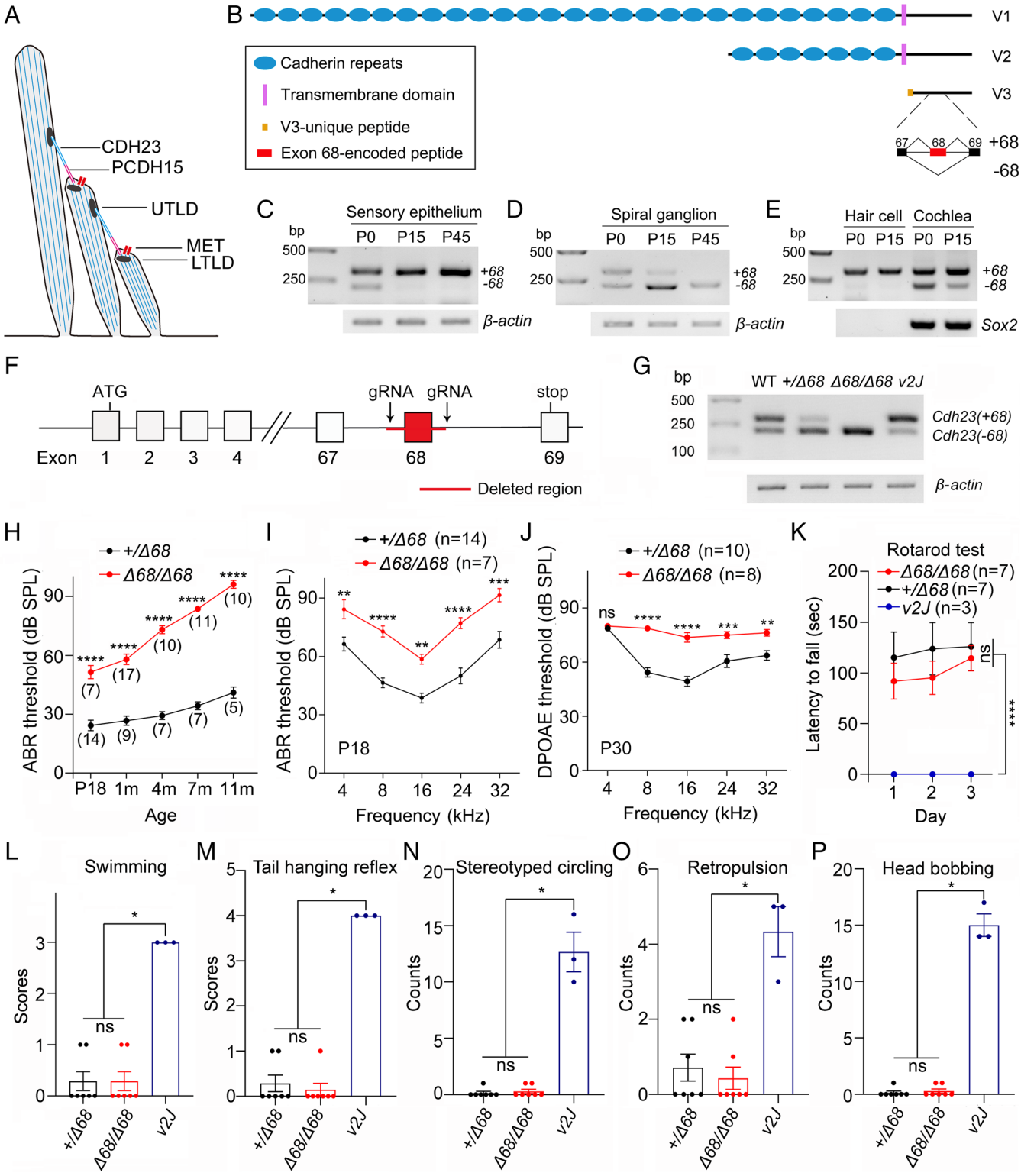

Fig. 1. *Cdh23*$^{\triangle 68/\triangle 68}$ mice show hearing loss but no balance deficits. (*A*) Schematic drawing of hair cell stereocilia and tip links. (*B*) Schematic drawing of various CDH23 isoforms. (*C* and *D*) RT-PCR results showing expression of *Cdh23(+68)* and *Cdh23(−68)* transcripts in mouse cochlear sensory epithelium (*C*) and spiral ganglion cells (*D*) at different ages as indicated. *β-actin* was included as an internal control. (*E*) RT-PCR results showing expression of *Cdh23(+68)* and *Cdh23(−68)* transcripts in mouse cochlea and isolated cochlear hair cells at P0 and P15. *Sox2* was included as an internal control for supporting cells. (*F*) Schematic drawing of the strategy for construction of *Cdh23* mutant mice with exon 68 deleted. Exons are indicated by numbered boxes. Deleted region is labeled in red. The positions of gRNA targets are indicated by arrows. (*G*) RT-PCR results showing expression of *Cdh23(+68)* and *Cdh23(−68)* transcripts in the cochlea from P5 wild-type (WT), *Cdh23*$^{+/\triangle 68}$, *Cdh23*$^{\triangle 68/\triangle 68}$, and *Cdh23*$^{v2J/v2J}$ mice. *β-actin* was included as an internal control. (*H*) ABR thresholds to click stimuli in *Cdh23*$^{+/\triangle 68}$ and *Cdh23*$^{\triangle 68/\triangle 68}$ mice of different ages as indicated. (*I*) ABR thresholds to pure tone stimuli in P18 *Cdh23*$^{+/\triangle 68}$ and *Cdh23*$^{\triangle 68/\triangle 68}$ mice. (*J*) DPOAE thresholds to pure tone stimuli in P30 *Cdh23*$^{+/\triangle 68}$ and *Cdh23*$^{\triangle 68/\triangle 68}$ mice. (*K–P*) Vestibular function of 7-month-old *Cdh23*$^{+/\triangle 68}$ and *Cdh23*$^{\triangle 68/\triangle 68}$ mice was evaluated by performing rotarod test (*K*), swimming test (*L*), tail hanging reflex (*M*), stereotyped circling movement (*N*), retropulsion (*O*), and head bobbing (*P*). *Cdh23*$^{v2J/v2J}$ mice were included as positive controls. The number of animals for each group is indicated in the brackets or by the number of symbols. The statistic test was performed via two-way ANOVA with Šídák's multiple comparisons test (for panels *H–J*), two-way ANOVA with Dunnett's multiple comparisons test (for panel *K*), or Kruskal–Wallis test with Dunn's multiple comparisons (for panels *L–P*). ns, not significant; *$P < 0.05$; **$P < 0.01$; ***$P < 0.001$; ****$P < 0.0001$.

harmonin (28). Immunoreactivity with an antibody against this exon 68-encoded peptide specifically localizes to the stereocilia, raising the possibility that CDH23(+68) might be the CDH23 isoform that forms tip links (10). However, the physiological significance of *Cdh23* exon 68 alternative splicing is unknown.

To explore the biological role of exon 68 splicing, we established mutant mice with *Cdh23* exon 68 deleted. Unexpectedly, tip links still form and function in young mutant mice, suggesting that CDH23(+68) is not essential for tip-link formation. However, deletion of exon 68 leads to loss of tip links and degeneration of shorter row mechanosensory stereocilia in aged mice or mice exposed to noise, suggesting that CDH23(+68) is required for the stability of tip links. Further investigations revealed that the exon 68-encoded peptide is necessary for dimerization of CDH23 as well as condensate formation with harmonin.

Results

CDH23 Isoforms Show Different Expression Patterns in the Mouse Cochlea. We first examined the expression pattern of *Cdh23(+68)* and *Cdh23(−68)* transcripts in mouse cochlea by performing RT-PCR. Both transcripts were readily detected in the sensory epithelium and spiral ganglion at postnatal day 0 (P0) (Fig. 1 *C* and *D*). However, at P15 and P45, *Cdh23(+68)* was predominantly detected in the sensory epithelium, whereas *Cdh23(−68)* was predominantly detected in the spiral ganglion (Fig. 1 *C* and *D*). We then isolated cochlear hair cells from *Atoh1*-GFP transgenic mice to examine *Cdh23* expression by RT-PCR. The results showed that *Cdh23(+68)* was predominantly expressed in P0 and P15 cochlear hair cells (Fig. 1*E*). Therefore, our present data are consistent with the hypothesis that CDH23(+68) is the main CDH23 isoform that forms tip links in cochlear hair cells.

We then employed injectoporation experiments to examine the localization of different CDH23 isoforms in cochlear hair cells. Expression vectors for different CDH23 isoforms with an HA tag at their C-termini were introduced into cochlear hair cells. Immunostaining with anti-HA antibody revealed that for the longest CDH23 isoform (V1), both CDH23(+68) and CDH23(−68) were localized to the stereocilia as well as in the cell body (*SI Appendix*, Fig. S1). For the second longest isoform (V2), both CDH23(+68) and CDH23(−68) were only detected in the cell body (*SI Appendix*, Fig. S1). Similar cytoplasmic localization was observed for the shortest isoform (V3) (*SI Appendix*, Fig. S1). As mentioned above, different from V1 and V2 isoforms that contain transmembrane segments, CDH23-V3 is a short, cytosolic protein, and adding a tag to its C terminus might affect its subcellular localization. Therefore, we added the HA tag to the N terminus of CDH23-V3, which was detected in the stereocilia as well as cell body in injectoporated hair cells (*SI Appendix*, Fig. S1). Together, our present data demonstrate that V1 and V3 isoforms of CDH23 can localize to the stereocilia.

Deletion of *Cdh23* Exon 68 Leads to Hearing Loss But No Balance Deficits. To investigate the function of *Cdh23* exon 68 splicing, we established mutant mice with *Cdh23* exon 68 deleted using the CRISPR/CRISPR-associated protein 9 genome editing technique (Fig. 1*F*). Sanger sequencing confirmed that a deletion of 218 bp including the entire exon 68 was introduced into the genome of the mutant mice (*SI Appendix*, Fig. S2 *A* and *B*). We generated the mutant mice on the C57BL/6 and CBA/CaJ mixed background but then back-crossed them to CBA/CaJ wild-type (WT) mice to generate heterozygous and eventually homozygous mutant mice. C57BL/6 but not CBA/CaJ mice carry the hypomorphic $Cdh23^{753A}$ allele that causes progressive hearing loss (30). Sanger sequencing revealed that the heterozygous and homozygous mutant mice only carried the $Cdh23^{753G}$ allele (*SI Appendix*, Fig. S2*C*), therefore excluding the effects of $Cdh23^{753A}$ on the phenotype of the mutant mice.

RT-PCR results confirmed that *Cdh23(+68)* was no longer expressed in the cochlea of the homozygous mutant ($Cdh23^{\triangle 68/\triangle 68}$) mice (Fig. 1*G*). Auditory brainstem response (ABR) measurements to click stimuli showed that there was a nearly 30 dB hearing threshold elevation in P18 $Cdh23^{\triangle 68/\triangle 68}$ mice compared to $Cdh23^{+/\triangle 68}$ mice (Fig. 1*H* and *SI Appendix*, Fig. S3*A*). The hearing threshold elevation was more pronounced in aged $Cdh23^{\triangle 68/\triangle 68}$ mice (Fig. 1*H* and *SI Appendix*, Fig. S3*A*). ABR measurements to pure tone stimuli revealed that hearing thresholds were elevated in $Cdh23^{\triangle 68/\triangle 68}$ mice at P18 and 4 mo of age at all frequencies examined (Fig. 1*I* and *SI Appendix*, Fig. S3 *B* and *C*). The ABR thresholds of $Cdh23^{+/\triangle 68}$ mice were indistinguishable from WT mice (*SI Appendix*, Fig. S3 *A–C*). Therefore, $Cdh23^{+/\triangle 68}$ mice were used as controls in the subsequent experiments. To examine outer hair cell (OHC) function in $Cdh23^{\triangle 68/\triangle 68}$ mice, we measured distortion product otoacoustic emissions (DPOAEs). DPOAE thresholds in $Cdh23^{\triangle 68/\triangle 68}$ mice at P30 were significantly elevated compared to $Cdh23^{+/\triangle 68}$ mice, suggesting that OHC function was compromised by *Cdh23* exon 68 deletion (Fig. 1*J*).

RT-PCR results also confirmed that *Cdh23(+68)* was no longer expressed in the vestibule of $Cdh23^{\triangle 68/\triangle 68}$ mice (*SI Appendix*, Fig. S4*A*). We evaluated the vestibular function of $Cdh23^{\triangle 68/\triangle 68}$ mice by performing rotarod test, swimming test, tail hanging test, stereotyped circling movement test, retropulsion test, and head bobbing test. $Cdh23^{v2J/v2J}$ mice were included as positive controls. As expected, $Cdh23^{v2J/v2J}$ mice showed severe balance deficits (22), whereas vestibular function in 7-month-old $Cdh23^{\triangle 68/\triangle 68}$ mice was unaffected (Fig. 1 *K–P*). Phalloidin staining and scanning electron microscopy (SEM) revealed no obvious morphological hair bundle defects in vestibular hair cells of $Cdh23^{\triangle 68/\triangle 68}$ mice (*SI Appendix*, Fig. S4 *B–D′*). Taken together, our data suggest that $Cdh23^{\triangle 68/\triangle 68}$ mice have hearing loss but preserved vestibular function.

Deletion of *Cdh23* Exon 68 Does Not Affect Tip-Link Formation or MET Function in Young Mice. CDH23 is a component of tip links, lateral links, and kinocilial links in developing hair cells (10, 13–16). In mature cochlear hair cells, however, CDH23 is mainly present in tip links, as lateral links and kinocilial links are transient structures that only exist in developing cochlear hair cells (6, 10, 12). We therefore examined tip links in mature cochlear hair cells of $Cdh23^{\triangle 68/\triangle 68}$ mice, initially by analyzing the expression of CDH23 using immunohistochemistry with a custom antibody that detects the CDH23(+68) and CDH23(−68) cytoplasmic tail. CDH23 was detected near the tips of stereocilia in control mice but not $Cdh23^{v2J/v2J}$ mice at P8, confirming the specificity of the antibody and the absence of tip links in $Cdh23^{v2J/v2J}$ mice (Fig. 2 *A* and *B*). Stereociliary tip localization of CDH23 was also observed in P8 $Cdh23^{\triangle 68/\triangle 68}$ mice, suggesting that tip-link formation was unaffected by *Cdh23* exon 68 deletion (Fig. 2 *A* and *B*). Next, we carried out SEM analysis to examine the shape of stereociliary tips. Beveled tips are thought to result from tip-link-mediated tension and are therefore a proxy for the presence of tip links (5, 7, 24, 31). We focused on the second-row stereocilia, whose relatively large dimension facilitates measurement of tip shape. Beveled second-row stereociliary tips were detected in the cochlear hair cells from P8 $Cdh23^{\triangle 68/\triangle 68}$ and control mice, but not in $Cdh23^{v2J/v2J}$ mice, suggesting that tip-link formation was not affected by *Cdh23* exon 68 deletion (Fig. 2 *C* and *D*). Lastly,

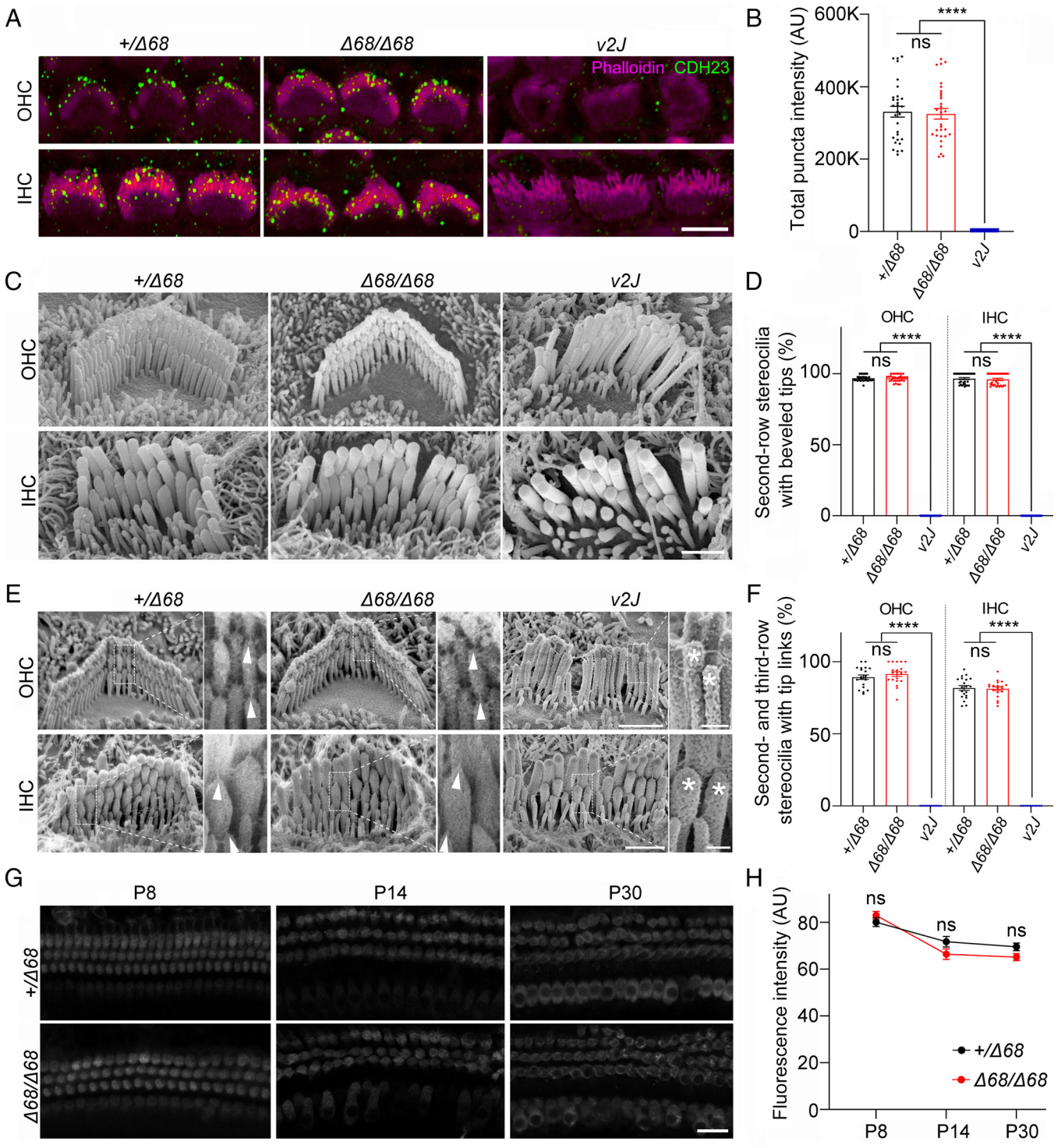

Fig. 2. Tip-link formation and FM1-43FX uptake are unaffected in young *Cdh23*$^{\triangle 68/\triangle 68}$ mice. (*A*) Localization of CDH23 in the stereocilia of P8 *Cdh23*$^{+/\triangle 68}$ and *Cdh23*$^{\triangle 68/\triangle 68}$ OHCs and IHCs was examined by performing whole-mount immunostaining using an antibody against the cytoplasmic tail of CDH23 (green). Stereociliary F-actin was visualized with TRITC-conjugated phalloidin (magenta). *Cdh23*$^{v2J/v2J}$ mice were included as negative controls. Shown are single confocal images taken from the middle cochlear turn. (*B*) Quantification of CDH23 immunoreactivity in the hair bundle per middle-turn OHC according to the whole-mount immunostaining results similar to *A*. (*C*) The morphology of hair bundles from P8 *Cdh23*$^{+/\triangle 68}$ and *Cdh23*$^{\triangle 68/\triangle 68}$ OHCs and IHCs was examined by SEM. *Cdh23*$^{v2J/v2J}$ mice were included as negative controls. Shown are single images taken from the middle cochlear turn. (*D*) Percentage of second-row stereocilia with beveled tips in middle-turn OHCs and IHCs was calculated from the SEM results similar to *C*. (*E*) Tip links of P8 *Cdh23*$^{+/\triangle 68}$ and *Cdh23*$^{\triangle 68/\triangle 68}$ OHCs and IHCs were examined by SEM. *Cdh23*$^{v2J/v2J}$ mice were included as negative controls. Shown are single images taken from the middle cochlear turn. Triangles indicate stereocilia with tip links; asterisks indicate stereocilia without tip links. (*F*) Percentage of second- and third-row stereocilia with tip links in middle-turn OHCs and IHCs was calculated from the SEM results similar to *E*. (*G*) FM1-43FX uptake by *Cdh23*$^{+/\triangle 68}$ and *Cdh23*$^{\triangle 68/\triangle 68}$ cochlear hair cells at different ages as indicated was examined using confocal microscope. Shown are single confocal images taken from the middle cochlear turn. (*H*) FM1-43FX uptake in middle-turn cochlear hair cells was quantified according to the results similar to *G*. (Scale bars, 5 μm in *A*, 1 μm in *C* and *E*, 200 nm in the *Insets* of *E*, and 10 μm in *G*.) The cell numbers for each group are indicated by the numbers of symbols (or 50 for panel *H*) from at least three animals. The statistic test was performed via one-way ANOVA with Dunnett's multiple comparisons test (for panel *B*, *F*, and OHCs in panel *D*), Kruskal–Wallis test with Dunn's multiple comparisons (for IHCs in panel *D*), or two-way ANOVA with Šídák's multiple comparisons test (for panel *H*). ns, not significant; ****$P < 0.0001$.

we directly quantified the numbers of tip links in SEM images, which showed that tip link numbers were comparable in control mice and *Cdh23*$^{\triangle 68/\triangle 68}$ mutants (Fig. 2 *E* and *F*).

Normal tip-link formation suggests that MET function might be preserved in young *Cdh23*$^{\triangle 68/\triangle 68}$ mice. To test this hypothesis, FM1-43FX dye uptake experiments were performed in mice of different genotypes. Up to P30, FM1-43FX dye uptake in *Cdh23*$^{\triangle 68/\triangle 68}$ hair cells was indistinguishable to that in control *Cdh23*$^{+/\triangle 68}$ hair cells (Fig. 2 *G* and *H*). We then recorded and quantified maximal MET currents by patch-clamping hair cells whose hair bundles were deflected with fluid jet. An averaged peak MET current of 697 ± 39 pA was recorded from P6-P8 *Cdh23*$^{\triangle 68/\triangle 68}$ OHCs, which is comparable to the current from control *Cdh23*$^{+/\triangle 68}$ OHCs (701 ± 21 pA) (Fig. 3 *A* and *B*). We also analyzed MET current kinetics from P6 to P8 OHCs in response to 10-ms bundle deflections ranging from −300 to 1,000 nm using a stiff probe (Fig. 3*C*). The activation and adaptation time constant of MET currents was not significantly different between *Cdh23*$^{\triangle 68/\triangle 68}$ and control *Cdh23*$^{+/\triangle 68}$ mice (Fig. 3 *C*–*F*). Lastly, we measured voltage-gated currents of OHCs, which again did not show any significant difference between *Cdh23*$^{\triangle 68/\triangle 68}$ and control *Cdh23*$^{+/\triangle 68}$ mice (Fig. 3 *G* and *H*). We conclude that MET function of cochlear hair cells was unaffected in young *Cdh23*$^{\triangle 68/\triangle 68}$ mice.

Deletion of *Cdh23* Exon 68 Causes Stereocilia Degeneration and OHC Loss in Adult Mice. ABR measurements revealed progressive hearing threshold elevation in *Cdh23*$^{\triangle 68/\triangle 68}$ mice (Fig. 1*H*). We then employed SEM to examine hair bundle morphology in *Cdh23*$^{\triangle 68/\triangle 68}$ mice at older ages. At 1 mo of age, the morphology of hair bundles in *Cdh23*$^{\triangle 68/\triangle 68}$ mice appeared largely normal (Fig. 4*A*). However, significant hair bundle loss was detected in 5-month-old *Cdh23*$^{\triangle 68/\triangle 68}$ OHCs, especially in the basal cochlear turn, which was further exaggerated in 8-month-old *Cdh23*$^{\triangle 68/\triangle 68}$ OHCs (Fig. 4 *A* and *B*). High-magnification SEM showed that degeneration of third-row stereocilia was detected in *Cdh23*$^{\triangle 68/\triangle 68}$ OHCs as early as P14, with increasing

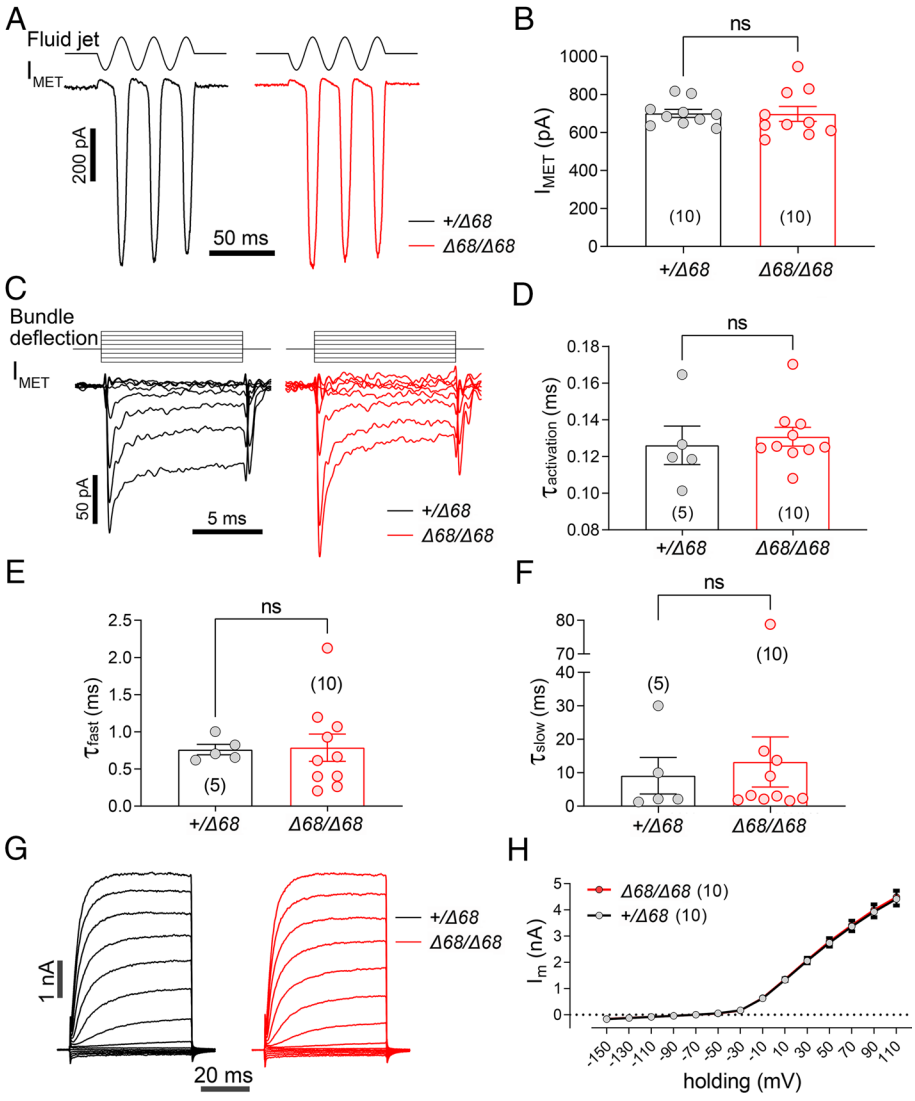

Fig. 3. MET currents are unaffected in young *Cdh23*$^{\triangle 68/\triangle 68}$ mice. (*A*) Representative MET currents induced by fluid jet were examined in OHCs from *Cdh23*$^{+/\triangle 68}$ and *Cdh23*$^{\triangle 68/\triangle 68}$ mice. A 40-Hz sinusoidal fluid jet was delivered to the hair bundle. (*B*) Averaged peak MET currents from similar data as shown in *A*. (*C*) Representative MET currents induced by a stiff probe were examined in OHCs from *Cdh23*$^{+/\triangle 68}$ and *Cdh23*$^{\triangle 68/\triangle 68}$ mice. A set of 10-ms-hair bundle deflections were delivered ranging from −300 nm to 1,000 nm at 100-nm steps. (*D*) Activation time constant ($\tau_{activation}$) in *Cdh23*$^{+/\triangle 68}$ OHCs (0.1261 ms) and *Cdh23*$^{\triangle 68/\triangle 68}$ OHCs (0.1308 ms). (*E*) Time constants of fast adaptation (τ_{fast}) in *Cdh23*$^{+/\triangle 68}$ OHCs (0.7614 ms) and *Cdh23*$^{\triangle 68/\triangle 68}$ OHCs (0.7868 ms). (*F*) Time constants of slow adaptation (τ_{slow}) in *Cdh23*$^{+/\triangle 68}$ OHCs (9.101 ms) and *Cdh23*$^{\triangle 68/\triangle 68}$ OHCs (13.22 ms). (*G*) Voltage-gated currents were recorded from *Cdh23*$^{+/\triangle 68}$ and *Cdh23*$^{\triangle 68/\triangle 68}$ OHCs. The membrane potential was altered from −150 mV to +110 mV at 20-mV steps. (*H*) I–V curves were drawn from data similar to panel (*G*). In all panels, data were collected from P6 to P8 OHCs from at least three mice with *Cdh23*$^{+/\triangle 68}$ shown in black and *Cdh23*$^{\triangle 68/\triangle 68}$ shown in red. Cell number is indicated in the brackets. The statistic test was performed via student's two-tailed unpaired *t* test. ns, not significant.

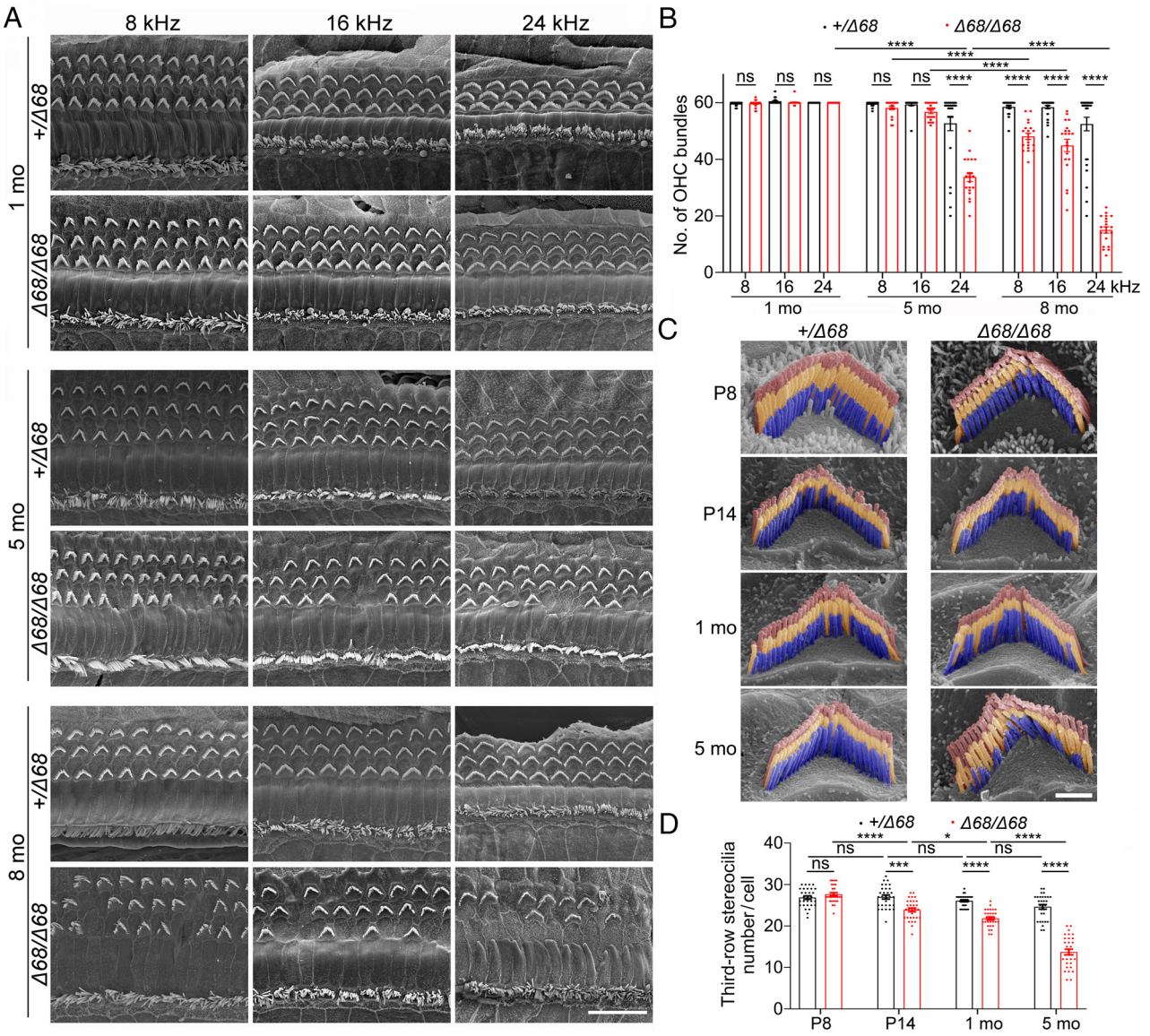

Fig. 4. Stereocilia maintenance is affected in adult *Cdh23*$^{\triangle 68/\triangle 68}$ cochlear hair cells. (*A*) Hair bundle morphology from *Cdh23*$^{+/\triangle 68}$ and *Cdh23*$^{\triangle 68/\triangle 68}$ mice at different ages and cochlear positions as indicated was examined by SEM. (*B*) OHC hair bundle numbers along successive 20-IHC intervals was calculated according to the SEM results similar to *A*. (*C*) High-magnification SEM images of middle-turn OHC hair bundles from *Cdh23*$^{+/\triangle 68}$ and *Cdh23*$^{\triangle 68/\triangle 68}$ mice at different ages as indicated. First-row stereocilia are indicated in red; second-row stereocilia are indicated in yellow; third-row stereocilia are indicated in blue. (*D*) Numbers of third-row stereocilia with normal height per OHC at middle cochlear turn was calculated according to the SEM results similar to *C*. (Scale bars, 20 μm in *A*, 1 μm in *C*.) The sample numbers for each group are indicated by the numbers of symbols from at least three animals. The statistic test was performed via two-way ANOVA with Tukey's multiple comparisons test. ns, not significant; **P* < 0.05; ****P* < 0.001; *****P* < 0.0001.

degeneration at subsequent ages (Fig. 4 *C* and *D*). Degeneration of third-row stereocilia was also observed in inner hair cells (IHCs) of *Cdh23*$^{\triangle 68/\triangle 68}$ mice at P14 (Fig. 5 *A* and *B*), albeit no complete hair bundle loss was detected in IHCs up to 8 mo (Fig. 4*A*).

Immunostaining with an antibody against the hair cell marker MYO7A revealed significant OHC loss in the basal cochlear turn of 5-month-old *Cdh23*$^{\triangle 68/\triangle 68}$ mice (*SI Appendix*, Fig. S5 *A*, *B*, and *D*). By 8 mo of age, OHC loss becomes more severe and extends to the apical cochlear turn in *Cdh23*$^{\triangle 68/\triangle 68}$ mice (*SI Appendix*, Fig. S5 *C* and *D*). Meanwhile, no significant IHC loss was detected in *Cdh23*$^{\triangle 68/\triangle 68}$ mice at any time points examined (*SI Appendix*, Fig. S5 *A*–*C*).

Adult *Cdh23*$^{\triangle 68/\triangle 68}$ Mice Show Decreased Tip-Link Numbers and Compromised MET. Degeneration of third-row mechanosensitive stereocilia might result from loss of tip links in adult *Cdh23*$^{\triangle 68/\triangle 68}$ mice. High-magnification SEM was then employed to examine beveled stereociliary tips and tip-link numbers in adult mice. Beveled second-row stereociliary tips were less prominent in 5-month-old *Cdh23*$^{\triangle 68/\triangle 68}$ IHCs (Fig. 5*C*), and tip-link numbers were significantly reduced in 8-month-old *Cdh23*$^{\triangle 68/\triangle 68}$ OHCs and IHCs (Fig. 5 *D* and *E*). Furthermore, the intensity of CDH23 immunoreactivity was decreased in 5-month-old *Cdh23*$^{\triangle 68/\triangle 68}$ OHCs (Fig. 5 *F* and *G*). Finally, FM1-43FX uptake was also decreased in 5-month-old *Cdh23*$^{\triangle 68/\triangle 68}$ cochlear hair cells (Fig. 5 *H* and *I*). Taken together, our data suggest that *Cdh23* exon 68 deletion affects the stability of tip links thus leading to tip-link loss as mice age, which in turn is expected to compromise MET and lead to hearing loss.

Deletion of *Cdh23* Exon 68 Leads to More Vulnerability to Noise-Induced Hearing Loss. Tip-link stability is affected by noise exposure that causes hearing loss (32, 33). We wanted to determine whether adult *Cdh23*$^{\triangle 68/\triangle 68}$ mice were more

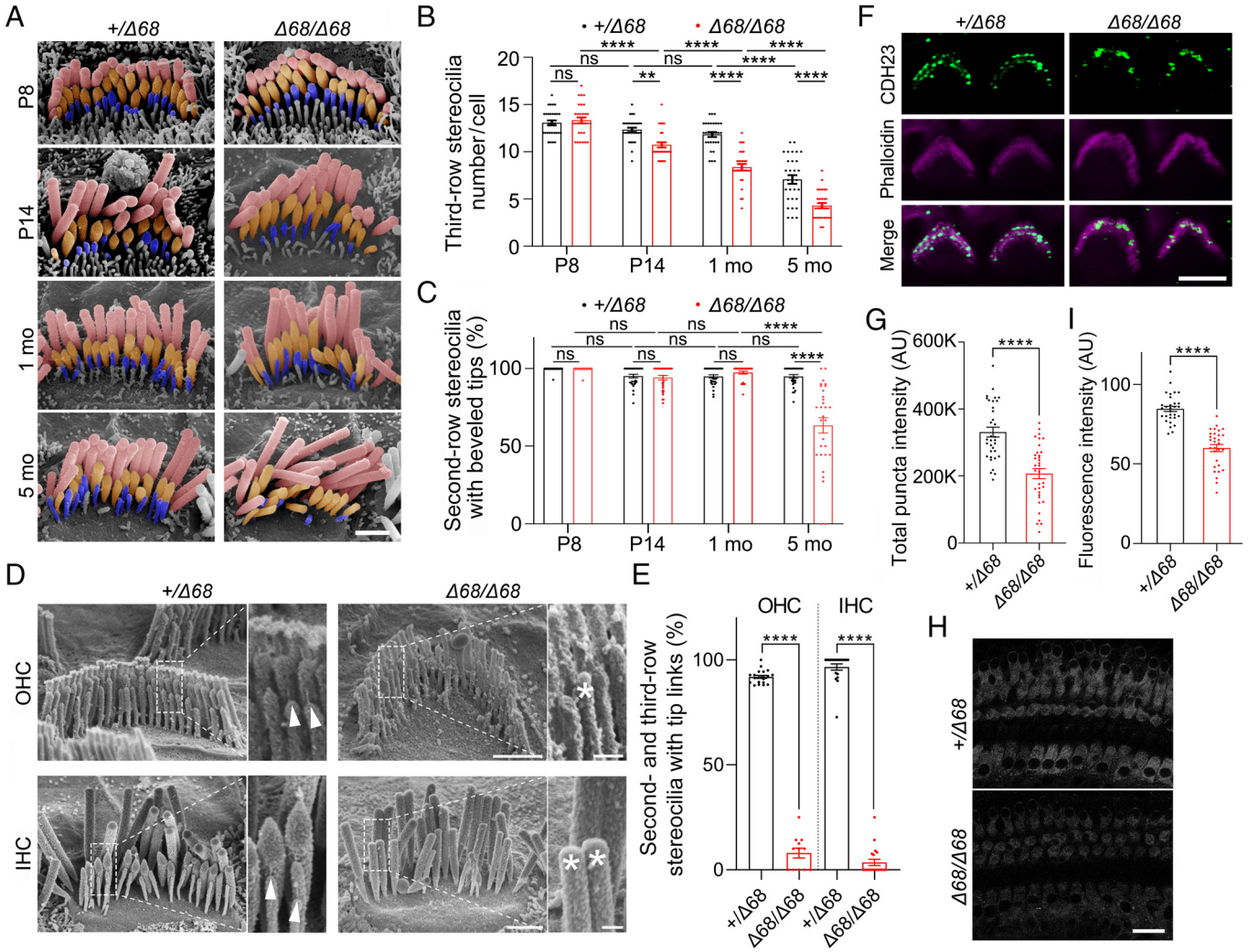

Fig. 5. Tip links and FM1-43FX uptake are affected in adult *Cdh23*$^{\triangle 68/\triangle 68}$ mice. (*A*) High-magnification SEM images of middle-turn IHC hair bundles from *Cdh23*$^{+/\triangle 68}$ and *Cdh23*$^{\triangle 68/\triangle 68}$ mice at different ages as indicated. First-row stereocilia are indicated in red; second-row stereocilia are indicated in yellow; third-row stereocilia are indicated in blue. (*B*) Numbers of third-row stereocilia with normal height per IHC at middle cochlear turn was calculated according to the SEM results similar to *A*. (*C*) Percentage of second-row stereocilia with beveled tips in middle-turn IHCs was calculated from the SEM results similar to *A*. (*D*) Tip links of 8-month-old *Cdh23*$^{+/\triangle 68}$ and *Cdh23*$^{\triangle 68/\triangle 68}$ OHCs and IHCs were examined by SEM. Shown are single images taken from the middle cochlear turn. Triangles indicate stereocilia with tip links; asterisks indicate stereocilia without tip links. (*E*) Percentage of second- and third-row stereocilia with tip links in middle-turn OHCs and IHCs was calculated from the SEM results similar to *D*. (*F*) Localization of CDH23 in the stereocilia of 5-month-old *Cdh23*$^{+/\triangle 68}$ and *Cdh23*$^{\triangle 68/\triangle 68}$ mice was examined by performing whole-mount immunostaining using an antibody against the cytoplasmic tail of CDH23 (green). Stereociliary F-actin was visualized with TRITC-conjugated phalloidin (magenta). Shown are single confocal images taken from the middle cochlear turn. (*G*) Quantification of CDH23 immunoreactivity in the hair bundle per middle-turn OHC according to the whole-mount immunostaining results similar to (*F*). (*H*) FM1-43FX uptake by 5-month-old *Cdh23*$^{+/\triangle 68}$ and *Cdh23*$^{\triangle 68/\triangle 68}$ cochlear hair cells was examined using confocal microscope. Shown are single images taken from the middle cochlear turn. (*I*) FM1-43FX uptake in middle-turn cochlear hair cells was quantified according to the results similar to *H*. (Scale bars, 1 μm in *A* and *D*, 200 nm in the *Insets* of *D*, 5 μm in *F*, and 10 μm in *H*.) The cell numbers for each group are indicated by the numbers of symbols from at least three animals. The statistic test was performed via two-way ANOVA with Tukey's multiple comparisons test (for panels *B* and *C*), Mann–Whitney test (for panel *E*), or student's *t* test (for panels *G* and *I*). ns, not significant; $^{**}P < 0.01$; $^{****}P < 0.0001$.

vulnerable to acoustic trauma. Exposure to a broadband noise of 2 to 20 kHz at 96 dB sound pressure level (SPL) for 2 h caused a temporary threshold shift (TTS) in *Cdh23*$^{+/\triangle 68}$ mice, with normal ABR thresholds restored 14 d later (Fig. 6 *A* and *B*). The same noise exposure paradigm led to greater, permanent threshold shift (PTS) in *Cdh23*$^{\triangle 68/\triangle 68}$ mice (Fig. 6 *A* and *B*). Consistently, SEM revealed that noise exposure induces enhanced OHC hair bundle loss in *Cdh23*$^{\triangle 68/\triangle 68}$ mice at both 1 d and 14 d after noise exposure (Fig. 6 *C* and *D*). High-magnification SEM further revealed significant degeneration of third-row stereocilia in *Cdh23*$^{\triangle 68/\triangle 68}$ OHCs (Fig. 6 *E* and *F*) and IHCs 14 d after exposure to noise (Fig. 7 *A* and *B*).

To our surprise, high-magnification SEM revealed that beveled second-row stereociliary tips in *Cdh23*$^{\triangle 68/\triangle 68}$ IHCs, similar to control *Cdh23*$^{+/\triangle 68}$ IHCs, were still present after noise exposure (Fig. 7*C*). Direct examination of tip links using SEM did not reveal a significant difference in the percentage of stereocilia with tip links between *Cdh23*$^{\triangle 68/\triangle 68}$ and control *Cdh23*$^{+/\triangle 68}$ mice 14 d after noise exposure (Fig. 7 *D* and *E*). However, CDH23 immunoreactivity was significantly decreased in *Cdh23*$^{\triangle 68/\triangle 68}$ mice at 1 d and 14 d after noise exposure (Fig. 7 *F* and *G*). In addition, FM1-43FX uptake was also significantly decreased in *Cdh23*$^{\triangle 68/\triangle 68}$ mice at 1 d and 14 d after noise exposure, suggesting of compromised MET function (Fig. 7 *H* and *I*). Taken together, our data suggest that *Cdh23*$^{\triangle 68/\triangle 68}$ mice are more vulnerable to acoustic trauma.

Exon 68 of CDH23 Affects Harmonin Condensate Formation. To gain insights into the mechanisms by which *Cdh23* alternative splicing regulates tip-link stability, we carried out biochemical experiments. It has been suggested that the exon 68-encoded

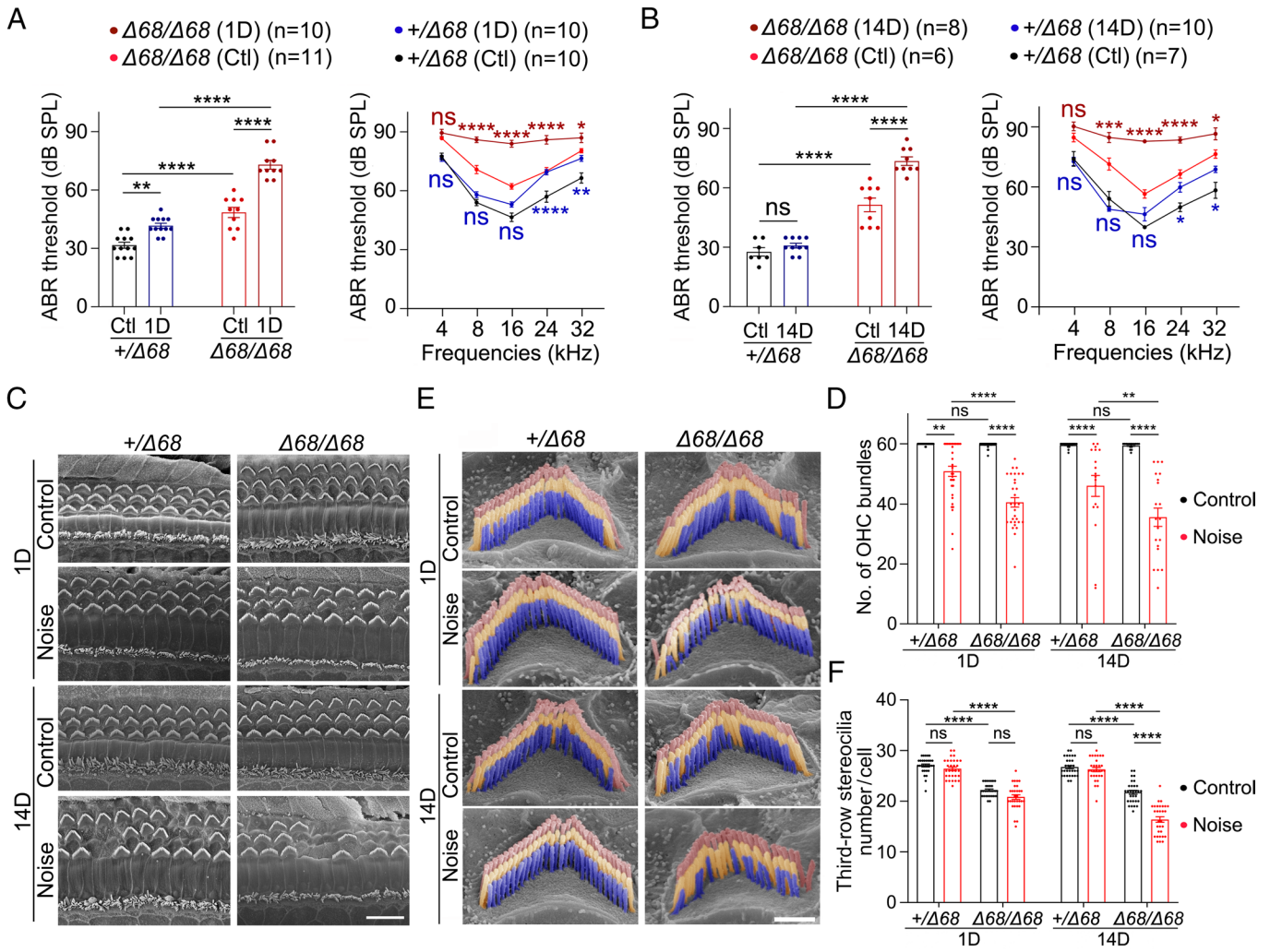

Fig. 6. *Cdh23*$^{\triangle 68/\triangle 68}$ mice show increased acoustic vulnerability. (*A* and *B*) One-month-old *Cdh23*$^{+/\triangle 68}$ and *Cdh23*$^{\triangle 68/\triangle 68}$ mice were exposed to a broadband noise of 2 to 20 kHz at 96 dB SPL for 2 h, and mice of the same genotypes and ages without noise exposure were included as control groups (Ctl). Hearing thresholds to pure tone or click stimuli 1 d (*A*) or 14 d (*B*) after noise treatment were analyzed by performing ABR measurements. (*C*) Hair bundle morphology from *Cdh23*$^{+/\triangle 68}$ and *Cdh23*$^{\triangle 68/\triangle 68}$ basal-turn hair cells at different time after noise exposure was examined by SEM. (*D*) OHC hair bundle numbers along successive 20-IHC intervals in the basal cochlear turn was calculated according to the SEM results similar to *C*. (*E*) High-magnification SEM images of middle-turn OHC hair bundles from *Cdh23*$^{+/\triangle 68}$ and *Cdh23*$^{\triangle 68/\triangle 68}$ mice at different time after noise exposure. First-row stereocilia are indicated in red; second-row stereocilia are indicated in yellow; third-row stereocilia are indicated in blue. (*F*) Numbers of third-row stereocilia with normal height per OHC in the middle cochlear turn was calculated according to the SEM results similar to *E*. (Scale bars, 10 μm in *C*, 1 μm in *E*.) The sample numbers for each group are indicated by the numbers of symbols from at least three animals. The statistic test was performed via two-way ANOVA with Tukey's multiple comparisons test (for panels *D* and *F* and click measurements in panels *A* and *B*), or two-way ANOVA with Šídák's multiple comparisons test (for pure-tune measurements in panels *A* and *B*). ns, not significant; **P* < 0.05; ***P* < 0.01; ****P* < 0.001; *****P* < 0.0001.

peptide induces dimerization of the cytoplasmic tail of CDH23 (34). Consistently, yeast two-hybrid and co-immunoprecipitation (co-IP) results showed that the cytoplasmic tail of CDH23(+68) but not CDH23(−68) mediates homo-dimerization (Fig. 8 *A* and *B*). Furthermore, sedimentation assays confirmed that the purified cytoplasmic tail of CDH23(+68) was more enriched in the pellet fraction than the cytoplasmic tail of CDH23(−68) (Fig. 8*C*).

The cytoplasmic tail of CDH23 interacts with harmonin, which has been suggested to participate in UTLD formation via phase separation together with MYO7A and SANS (27, 28, 35–37). We therefore determined whether *Cdh23* exon 68 splicing affects condensate formation of CDH23 and harmonin. The longest harmonin isoform (harmonin-b) contains a N-terminal domain (NTD), three PDZ domains, two coiled-coil domains, and a proline, serine, and threonine-rich domain. Harmonin binds to the cytoplasmic tail of CDH23 through its NTD and the second PDZ domain (PDZ2) (25, 28, 35, 36). Therefore, we performed co-sedimentation assays with the purified CDH23 cytoplasmic tail and harmonin NPDZ12 fragment that contains the NTD and the first two PDZ domains. CDH23(+68) predominantly co-sedimented with the harmonin NPDZ12 fragment (Fig. 8*D*). When the Cy3-labeled CDH23(+68) cytoplasmic tail was mixed with Alexa 488-labeled harmonin NPDZ12 fragment, significant spherical droplets with enrichment of both proteins were observed by fluorescence microscopy (Fig. 8*E*). Moreover, these droplets formed in a dose-dependent manner (Fig. 8*F*). In contrast, the CDH23(−68) cytoplasmic tail barely formed large droplets with the harmonin NPDZ12 fragment (Fig. 8 *E* and *F*). We then conducted fluorescence recovery after photobleaching assay to evaluate the mobility of CDH23(+68) cytoplasmic tail within the droplets. Within 8 min after photobleaching, only 20 to 40% of the fluorescence signal recovered (Fig. 8 *G* and *H*), suggesting that CDH23(+68) cytoplasmic tail forms solid-like condensates with harmonin. Taken together, our results provide evidence that exon 68 of CDH23 plays a role in the assembly of condensates involving harmonin.

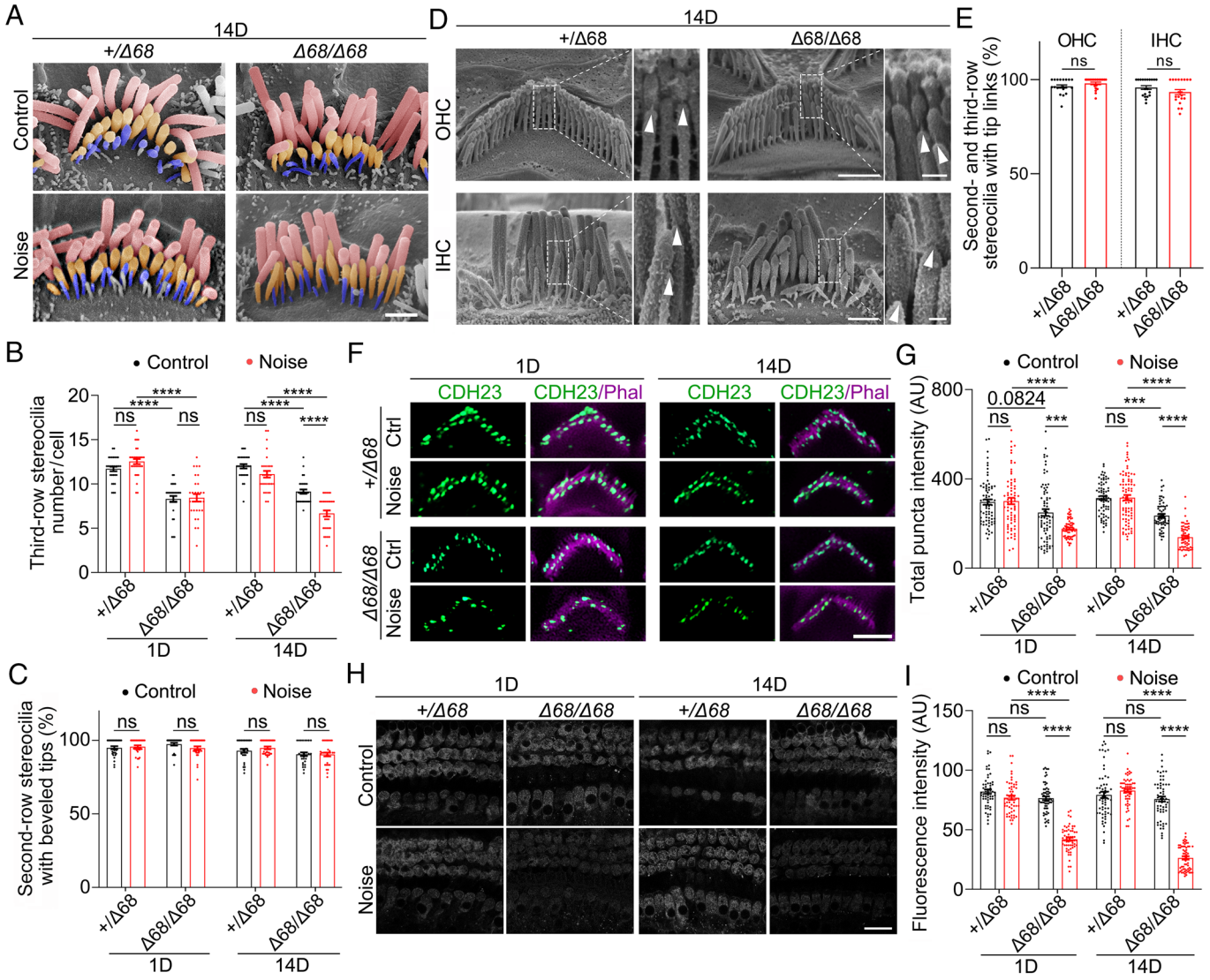

Fig. 7. Stereocilia maintenance and FM1-43FX uptake are affected in noise-exposed *Cdh23*$^{\triangle 68/\triangle 68}$ mice. (*A*) High-magnification SEM images of middle-turn IHC hair bundles from *Cdh23*$^{+/\triangle 68}$ and *Cdh23*$^{\triangle 68/\triangle 68}$ mice 14 d after noise exposure. First-row stereocilia are indicated in red; second-row stereocilia are indicated in yellow; third-row stereocilia are indicated in blue. (*B*) Numbers of third-row stereocilia with normal height per IHC in the middle cochlear turn was calculated according to the SEM results similar to *A*. (*C*) Percentage of second-row stereocilia with beveled tips in middle-turn hair cells was calculated from the SEM results similar to *A*. (*D*) Tip links of *Cdh23*$^{+/\triangle 68}$ and *Cdh23*$^{\triangle 68/\triangle 68}$ OHCs and IHCs at 14 d after noise exposure were examined by SEM. Shown are single images taken from the middle cochlear turn. Triangles indicate stereocilia with tip links. (*E*) Percentage of second- and third-row stereocilia with tip links in middle-turn hair cells at 14 d after noise was calculated from the SEM results similar to *D*. (*F*) Localization of CDH23 in the stereocilia of *Cdh23*$^{+/\triangle 68}$ and *Cdh23*$^{\triangle 68/\triangle 68}$ mice at different times after noise exposure was examined by performing whole-mount immunostaining using an antibody against the cytoplasmic tail of CDH23 (green). Stereociliary F-actin was visualized with TRITC-conjugated phalloidin (magenta). Shown are single confocal images taken from the middle cochlear turn. (*G*) Quantification of CDH23 immunoreactivity in the hair bundle per middle-turn OHC according to the whole-mount immunostaining results similar to *F*. (*H*) FM1-43FX uptake by *Cdh23*$^{+/\triangle 68}$ and *Cdh23*$^{\triangle 68/\triangle 68}$ cochlear hair cells at different times after noise exposure was examined using a confocal microscope. Shown are single images taken from the middle cochlear turn. (*I*) FM1-43FX uptake in middle-turn hair cells was quantified according to the results similar to *H*. (Scale bars, 1 μm in *A* and *D*, 200 nm in the *Insets* of *D*, 2.5 μm in *F*, and 10 μm in *H*.) The cell numbers for each group are indicated by the numbers of symbols from at least three animals. The statistic test was performed via two-way ANOVA with Tukey's multiple comparisons test (for panels *B*, *C*, *G*, and *I*) or Mann–Whitney test (for panel *E*). ns, not significant; ***$P < 0.001$; ****$P < 0.0001$.

Discussion

About the alternative splicing of *Cdh23* exon 68, two intriguing questions have remained unanswered for many years. First, how is this inner ear-specific splicing regulated? Second, what is the biological significance of this alternative splicing? Our recent work provided the answer to the first question. Through cell-based screening, we found that alternative splicing of *Cdh23* exon 68 is promoted by RBM24 and RBM38 and inhibited by PTBP1 (38). Moreover, the inclusion of *Cdh23* exon 68 is almost completely abolished in the cochlea of *Rbm24* knockout mice (39). Our present work now provides insights into the answer to the second question. Our data suggest that *Cdh23* exon 68 is important for maintaining the stability of tip links through regulating UTLD formation.

Our RT-PCR results showed that the *Cdh23(+68)* transcript is predominantly expressed in postnatal cochlear hair cells, implying that CDH23(+68) but not CDH23(−68) is the main CDH23 isoform that forms tip links in mature hair cells. Surprisingly, the formation and function of tip links are largely unaffected in young mice with *Cdh23* exon 68 deleted. Several lines of evidence support this conclusion. First, CDH23 immunoreactivity in the stereocilia is unaffected in young *Cdh23*$^{\triangle 68/\triangle 68}$ mice. Second, beveled stereociliary tips, an indicator of the presence of functional tip links, are unaffected in young *Cdh23*$^{\triangle 68/\triangle 68}$ mice. Third, tip links directly examined using SEM are unaffected in young *Cdh23*$^{\triangle 68/\triangle 68}$ mice.

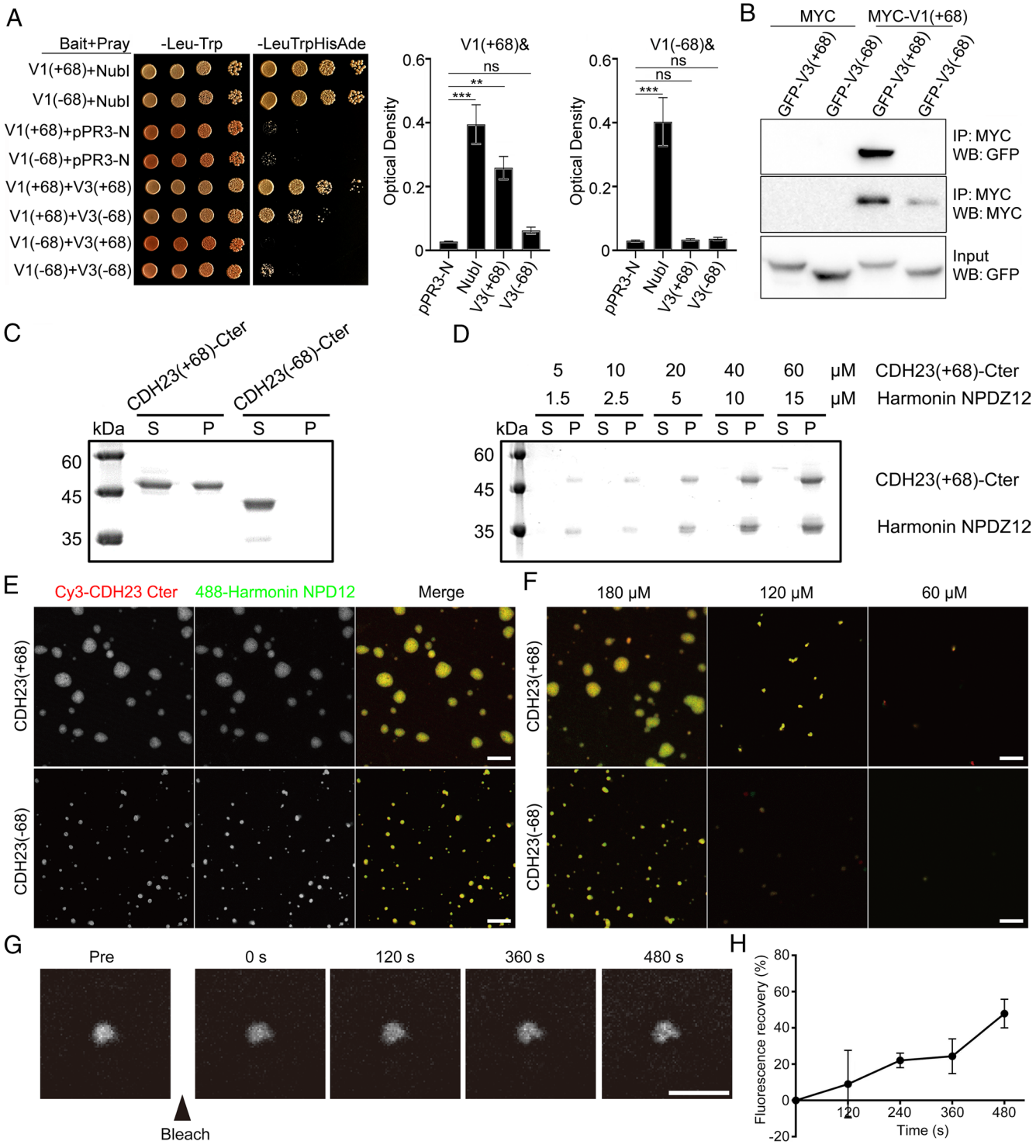

Fig. 8. Exon 68 is important for CDH23 dimerization and condensate formation. (*A*) Interaction between CDH23 isoforms examined by performing yeast two-hybrid assay. (*Left*) Transformation efficiency is examined on SD-Leu-Trp medium, and protein–protein interaction is examined on SD-Leu-Trp-His-Ade medium. (*Right*) Quantification of protein–protein interaction according to results similar to *Left*. Nubl and pPR3-N are included as positive and negative controls, respectively. (*B*) Interaction between CDH23 isoforms examined by co-IP. Expression vectors were transfected into HEK293T cells to express GFP- or MYC-tagged CDH23 isoforms, and cell lysates were subjected to immunoprecipitation. IP indicates antibody used for immunoprecipitation, and WB indicates antibody used for detection. (*C*) Sedimentation results of CDH23 cytoplasmic tail (50 μM) showing that CDH23(+68) cytoplasmic tail was more enriched in the pellet than CDH23(−68) cytoplasmic tail. S indicates supernatant, and P indicates pellet. (*D*) Co-sedimentation results of CDH23(+68) cytoplasmic tail mixed with harmonin NPDZ12 fragment. Both proteins were enriched in the pellet and the pellet fraction of the mixture exceeds that of CDH23(+68) cytoplasmic tail alone. (*E*) Fluorescent images showing that CDH23(+68) cytoplasmic tail/harmonin NPDZ12 fragment forms larger droplets than CDH23(−68) cytoplasmic tail/harmonin NPDZ12 fragment. CDH23 cytoplasmic tail and harmonin NPDZ12 fragment were labeled with Cy3 and Alexa 488, respectively. Labeled proteins were added at a ratio of 1%. CDH23 cytoplasmic tail: 180 μM, harmonin NPDZ12 fragment: 45 μM. (*F*) Fluorescent images showing that the phase separation capacity of CDH23 cytoplasmic tail/harmonin NPDZ12 fragment is concentration-dependent. The concentration ratio of CDH23 cytoplasmic tail: harmonin NPDZ12 fragment is 4:1, and proteins were labeled in the same way as in *E*. The concentration of CDH23 cytoplasmic tail was indicated. (*G*) Images showing the recovery process of CDH23(+68) cytoplasmic tail fluorescence after photobleaching. Proteins were labeled in the same way as in *E*. (*H*) Quantification of the recovery process of CDH23(+68) cytoplasmic tail fluorescence according to results similar to *G* (n = 3). (Scale bars, 10 μm in *E* and *F*, 5 μm in *G*.) The statistic test was performed via one-way ANOVA with Dunnett's multiple comparisons test (for panel *A*). ns, not significant; $^{**}P < 0.01$; $^{***}P < 0.001$.

Fourth, *Cdh23* exon 68 deletion in young mice does not affect FM1-43FX dye uptake, an indicator of functional integrity of hair cells. Last, the electrophysiology results confirmed that *Cdh23* exon 68 deletion does not affect MET in young mice. Together, our present data reveal that albeit tip links are mainly formed by CDH23(+68) in native hair cells, CDH23(−68) could fulfill this function when CDH23(+68) is absent.

However, the CDH23(−68)-containing tip links are less stable than CDH23(+68)-containing tip links. It has been shown that tip links are sensitive to aging and environmental insults such as noise (23, 32, 40). Our data reveal that the number of tip links is significantly decreased in aged $Cdh23^{\triangle 68/\triangle 68}$ mice. Moreover, aged $Cdh23^{\triangle 68/\triangle 68}$ mice show robust stereocilia degeneration and reduced FM1-43FX dye uptake. Consistently, $Cdh23^{\triangle 68/\triangle 68}$ mice manifest progressive hearing loss. Therefore, our present data suggest that deletion of *Cdh23* exon 68 affects the stability of tip links, and eventually contributes to progressive hearing loss. Inclusion of *Cdh23* exon 68 happens in both the cochlea and vestibula. However, in contrast to hearing loss, no balance deficits could be detected in $Cdh23^{\triangle 68/\triangle 68}$ mice up to 7 mo of age. Compared to cochlear stereocilia, vestibular stereocilia are subjected to less intense daily stimuli, which might explain why tip links in vestibular hair cells are more stable even when exon 68 is absent.

When exposed to noise stimuli that lead to TTS in control mice, $Cdh23^{\triangle 68/\triangle 68}$ mice manifest PTS with greater threshold elevation. Enhanced stereocilia degeneration and reduced FM1-43FX dye uptake were also observed in noise-exposed $Cdh23^{\triangle 68/\triangle 68}$ mice. However, tip links associated with the remained stereocilia were largely unaffected when examined 1 d or 14 d after noise exposure. It has been suggested that tip links recover within seconds to hours after disruption by Ca^{2+} chelation (41–43). It's tempting to speculate that tip-link recovery might also happen quickly in a similar time scale after noise exposure, which explains why we did not detect tip-link loss in noise-exposed mice. Nevertheless, the temporary tip-link loss might lead to stereocilia degeneration, which could not be restored easily and eventually contribute to the observed noise-induced hearing loss. Consistent with this hypothesis, loss of tip links could only be detected in adult $Cdh23^{\triangle 68/\triangle 68}$ mice at rather late age.

Further investigation showed that the CDH23(+68) cytoplasmic tail is more prone to dimerize and form condensates than the CDH23(−68) cytoplasmic tail. It has been shown that the cytoplasmic tail of CDH23, as well as harmonin, MYO7A, and SANS interact with each other and form a so-called UTLD protein complex at the upper insertion site of tip links (5, 24–26). In line with this, harmonin, MYO7A, and SANS form condensates via phase separation (27). Moreover, the CDH23(+68) cytoplasmic tail and harmonin form large protein assemblies through multivalent interactions (34). Our present data confirm that the cytoplasmic tail of CDH23(+68) but not CDH23(−68) dimerize and form condensates together with harmonin, suggesting that the CDH23(+68) cytoplasmic tail might contribute to the formation of the UTLD. Our data also imply that the CDH23 short isoform (CDH23-V3) might play an important role in this process. CDH23-V3(+68) can bind to CDH23-V1(+68), and therefore might contribute to the formation of a large protein condensate near the upper end of tip links through multivalent interactions with other UTLD components (*SI Appendix*, Fig. S6).

Hearing threshold elevation was observed as early as P18 in $Cdh23^{\triangle 68/\triangle 68}$ mice, by which time stereocilia morphology was largely normal except some degeneration of third-row stereocilia, and MET function revealed by FM1-43FX uptake was also not significantly affected. Therefore, cochlear function that does not involve tip links and even stereocilia might be compromised by *Cdh23* exon 68 deletion. It has been shown that ribbon synapse numbers are significantly reduced in aged C57BL/6N mice that carry the hypomorphic $Cdh23^{753A}$ allele, and repair of this mutation partially rescues the phenotype (44, 45). Further investigations are warranted to fully understand the mechanisms that lead to the synaptic defects.

Materials and Methods

Animal experiments were approved by the Animal Ethics Committee of Shandong University School of Life Sciences (Permit Number: SYDWLL-2021-74) and performed accordingly. *Animal Models*, *Hair Cell Isolation and RT-PCR*, *Injectoporation*, *Whole-Mount Immunostaining*, *ABR Measurement*, *DPOAE Measurement*, *Vestibular Function Examination*, *FM1-43FX Uptake Experiment*, *SEM*, *Electrophysiology*, *Noise Exposure*, *Yeast Two-Hybrid*, *Co-IP and Western Blot*, *Protein Purification and Sedimentation Assay*, *Protein Labeling and Fluorescent Imaging*, *FRAP Analysis*, and *Statistical Analysis* are described in *SI Appendix, SI Materials and Methods*.

Data, Materials, and Software Availability. All study data are included in the article and/or *SI Appendix*.

ACKNOWLEDGMENTS. We thank Sen Wang, Yuyu Guo, Xiaomin Zhao, and Haiyan Yu from the core facilities for life and environmental sciences, Shandong University for technical support in SEM and confocal microscopy. We thank Dr. Tao Yang and Longhao Wang from Shanghai Jiao Tong University School of Medicine for the advises in SEM. This work was supported by grants from National Key Research & Developmental Program of China (2022YFE0131900), National Natural Science Foundation of China (82192861, 82071051), China Ministry of Science and Technology (2021ZD0203304), and Shandong Provincial Natural Science Foundation (ZR2020ZD39).

Author affiliations: [a]Shandong Provincial Key Laboratory of Animal Cells and Developmental Biology and Key Laboratory for Experimental Teratology of the Ministry of Education, School of Life Sciences, Shandong University, Qingdao, Shandong 266237, China; [b]Chinese Institute for Brain Research, Beijing 102206, China; [c]Key Laboratory for the Genetics of Developmental and Neuropsychiatric Disorders, Ministry of Education, Bio-X Institutes, Shanghai Jiao Tong University, Shanghai 200030, China; [d]The Solomon H. Snyder Department of Neuroscience, Johns Hopkins University School of Medicine, Baltimore, MD 21205; and [e]Shandong Provincial Collaborative Innovation Center of Cell Biology, Shandong Normal University, Jinan, Shandong 250014, China

1. K. Kikuchi, D. Hilding, The development of the organ of Corti in the mouse. *Acta Otolaryngol.* **60**, 207–222 (1965).
2. A. J. Hudspeth, R. Jacobs, Stereocilia mediate transduction in vertebrate hair cells (auditory system/cilium/vestibular system). *Proc. Natl. Acad. Sci. U.S.A.* **76**, 1506–1509 (1979).
3. C. Jones *et al.*, Ciliary proteins link basal body polarization to planar cell polarity regulation. *Nat. Genet.* **40**, 69–77 (2008).
4. J. O. Pickles, S. D. Comis, M. P. Osborne, Cross-links between stereocilia in the guinea pig organ of Corti, and their possible relation to sensory transduction. *Hear. Res.* **15**, 103–112 (1984).
5. D. N. Furness, C. M. Hackney, Cross-links between stereocilia in the guinea-pig cochlea. *Hear. Res.* **18**, 177–188 (1985).
6. R. J. Goodyear, W. Marcotti, C. J. Kros, G. P. Richardson, Development and properties of stereociliary link types in hair cells of the mouse cochlea. *J. Comp. Neurol.* **485**, 75–85 (2005).
7. J. A. Assad, G. M. Shepherd, D. P. Corey, Tip-link integrity and mechanical transduction in vertebrate hair cells. *Neuron* **7**, 985–994 (1991).
8. M. Beurg, R. Fettiplace, J. H. Nam, A. J. Ricci, Localization of inner hair cell mechanotransducer channels using high-speed calcium imaging. *Nat. Neurosci.* **12**, 553–558 (2009).
9. X. Qiu, U. Müller, Sensing sound: Cellular specializations and molecular force sensors. *Neuron* **110**, 3667–3687 (2022).
10. J. Siemens *et al.*, Cadherin 23 is a component of the tip link in hair-cell stereocilia. *Nature* **428**, 950–955 (2004).
11. Z. M. Ahmed *et al.*, The tip-link antigen, a protein associated with the transduction complex of sensory hair cells, is protocadherin-15. *J. Neurosci.* **26**, 7022–7034 (2006).
12. P. Kazmierczak *et al.*, Cadherin 23 and protocadherin 15 interact to form tip-link filaments in sensory hair cells. *Nature* **449**, 87–91 (2007).
13. A. Lagziel *et al.*, Spatiotemporal pattern and isoforms of cadherin 23 in wild type and waltzer mice during inner ear hair cell development. *Dev. Biol.* **280**, 295–306 (2005).
14. V. Michel *et al.*, Cadherin 23 is a component of the transient lateral links in the developing hair bundles of cochlear sensory cells. *Dev. Biol.* **280**, 281–294 (2005).

15. A. K. Rzadzinska, A. Derr, B. Kachar, K. Noben-Trauth, Sustained cadherin 23 expression in young and adult cochlea of normal and hearing-impaired mice. *Hear. Res.* **208**, 114–121 (2005).
16. R. J. Goodyear, A. Forge, P. K. Legan, G. P. Richardson, Asymmetric distribution of cadherin 23 and protocadherin 15 in the kinocilial links of avian sensory hair cells. *J. Comp. Neurol.* **518**, 4288–4297 (2010).
17. H. Bolz *et al.*, Mutation of CDH23, encoding a new member of the cadherin gene family, causes Usher syndrome type 1D. *Nat. Genet.* **27**, 108–112 (2001).
18. J. M. Bork *et al.*, Usher syndrome 1D and nonsyndromic autosomal recessive deafness DFNB12 are caused by allelic mutations of the novel cadherin-like gene CDH23. *Am. J. Hum. Genet.* **68**, 26–37 (2001).
19. Z. M. Ahmed *et al.*, Mutations of the protocadherin gene PCDH15 cause Usher syndrome type 1F. *Am. J. Hum. Genet.* **69**, 25–34 (2001).
20. K. N. Alagramam *et al.*, Mutations in the novel protocadherin PCDH15 cause Usher syndrome type 1F. *Hum. Mol. Genet.* **10**, 1709–1718 (2001).
21. K. N. Alagramam *et al.*, The mouse Ames waltzer hearing-loss mutant is caused by mutation of Pcdh15, a novel protocadherin gene. *Nat. Genet.* **27**, 99–102 (2001).
22. F. Di Palma *et al.*, Mutations in Cdh23, encoding a new type of cadherin, cause stereocilia disorganization in waltzer, the mouse model for Usher syndrome type 1D. *Nat. Genet.* **27**, 103–107 (2001).
23. M. Schwander *et al.*, A mouse model for nonsyndromic deafness (DFNB12) links hearing loss to defects in tip links of mechanosensory hair cells. *Proc. Natl. Acad. Sci. U.S.A.* **106**, 5252–5257 (2009).
24. B. Kachar, M. Parakkal, M. Kurc, Y. Zhao, P. G. Gillespie, High-resolution structure of hair-cell tip links. *Proc. Natl. Acad. Sci. U.S.A.* **97**, 13336–13341 (2000).
25. N. Grillet *et al.*, Harmonin mutations cause mechanotransduction defects in cochlear hair cells. *Neuron* **62**, 375–387 (2009).
26. M. Grati, B. Kachar, Myosin VIIa and sans localization at stereocilia upper tip-link density implicates these Usher syndrome proteins in mechanotransduction. *Proc. Natl. Acad. Sci. U.S.A.* **108**, 11476–11481 (2011).
27. Y. He, J. Li, M. Zhang, Myosin VII, USH1C, and ANKS4B or USH1G together form condensed molecular assembly via liquid-liquid phase separation. *Cell Rep.* **29**, 974–986 (2019).
28. J. Siemens *et al.*, The Usher syndrome proteins cadherin 23 and harmonin form a complex by means of PDZ-domain interactions. *Proc. Natl. Acad. Sci. U.S.A.* **99**, 14946–14951 (2002).
29. Z. Xu, A. W. Peng, K. Oshima, S. Heller, MAGI-1, a candidate stereociliary scaffolding protein, associates with the tip-link component Cadherin 23. *J. Neurosci.* **28**, 11269–11276 (2008).
30. K. Noben-Trauth, Q. Zheng, K. R. Johnson, Association of cadherin 23 with polygenic inheritance and genetic modification of sensorineural hearing loss. *Nat. Genet.* **35**, 21–23 (2003).
31. J. O. Pickles, G. W. Rouse, M. von Perger, Morphological correlates of mechanotransduction in acousticolateral hair cells. *Scan. Microsc.* **5**, 1115–1128 (1991).
32. J. O. Pickles, M. P. Osborne, S. D. Comis, Vulnerability of tip links between stereocilia to acoustic trauma in the guinea-pig. *Hear. Res.* **25**, 173–183 (1987).
33. M. Takumida, L. Fredelius, D. Bagger-Sjoback, Y. Harada, J. Wersall, Effect of acoustic overstimulation on the glycocalyx and the ciliary interconnections in the organ of Corti: High resolution scanning electron microscopic investigation. *J. Laryngol. Otol.* **103**, 1125–1129 (1989).
34. L. Wu, L. Pan, C. Zhang, M. Zhang, Large protein assemblies formed by multivalent interactions between cadherin23 and harmonin suggest a stable anchorage structure at the tip link of stereocilia. *J. Biol. Chem.* **287**, 33460–33471 (2012).
35. B. Boeda *et al.*, Myosin VIIa, harmonin and cadherin 23, three Usher I gene products that cooperate to shape the sensory hair cell bundle. *EMBO J.* **21**, 6689–6699 (2002).
36. L. Pan, J. Yan, L. Wu, M. Zhang, Assembling stable hair cell tip link complex via multidentate interactions between harmonin and cadherin 23. *Proc. Natl. Acad. Sci. U.S.A.* **106**, 5575–5580 (2009).
37. A. Bahloul *et al.*, Cadherin-23, myosin VIIa and harmonin, encoded by Usher syndrome type I genes, form a ternary complex and interact with membrane phospholipids. *Hum. Mol. Genet.* **19**, 3557–3565 (2010).
38. N. Li, H. Du, R. Ren, Y. Wang, Z. Xu, Alternative splicing of Cdh23 exon 68 is regulated by RBM24, RBM38, and PTBP1. *Neural Plast.* **2020**, 8898811 (2020).
39. Y. Wang *et al.*, RBM24 is required for mouse hair cell development through regulating pre-mRNA alternative splicing and mRNA stability. *J. Cell. Physiol.* **238**, 1095–1110 (2023).
40. J. M. Husbands, S. A. Steinberg, R. Kurian, J. C. Saunders, Tip-link integrity on chick tall hair cell stereocilia following intense sound exposure. *Hear. Res.* **135**, 135–145 (1999).
41. Y. Zhao, E. N. Yamoah, P. G. Gillespie, Regeneration of broken tip links and restoration of mechanical transduction in hair cells. *Proc. Natl. Acad. Sci. U.S.A.* **93**, 15469–15474 (1996).
42. A. A. Indzhykulian *et al.*, Molecular remodeling of tip links underlies mechanosensory regeneration in auditory hair cells. *PLoS Biol.* **11**, e1001583 (2013).
43. R. G. Alonso, M. Tobin, P. Martin, A. J. Hudspeth, Fast recovery of disrupted tip links induced by mechanical displacement of hair bundles. *Proc. Natl. Acad. Sci. U.S.A.* **117**, 30722–30727 (2020).
44. J. Mianne *et al.*, Correction of the auditory phenotype in C57BL/6N mice via CRISPR/Cas9-mediated homology directed repair. *Genome Med.* **8**, 16 (2016).
45. J. Jeng *et al.*, Pathophysiological changes in inner hair cell ribbon synapses in the ageing mammalian cochlea. *J. Physiol.* **598**, 4339–4355 (2020).